

Transformable peptide nanoparticles arrest HER2 signalling and cause cancer cell death in vivo

Lu Zhang^{1,6}, Di Jing^{1,6}, Nian Jiang^{2,3}, Tatu Rojalin¹, Christopher M. Baehr¹, Dalin Zhang¹, Wenwu Xiao¹, Yi Wu¹, Zhaoqing Cong¹, Jian Jian Li², Yuanpei Li¹, Lei Wang^{4*} and Kit S. Lam^{1,5*}

Human epidermal growth factor receptor 2 (HER2) is overexpressed in >20% of breast cancers. Dimerization of HER2 receptors leads to the activation of downstream signals enabling the proliferation and survival of malignant phenotypes. Owing to the high expression levels of HER2, combination therapies are currently required for the treatment of HER2⁺ breast cancer. Here, we designed non-toxic transformable peptides that self-assemble into micelles under aqueous conditions but, on binding to HER2 on cancer cells, transform into nanofibrils that disrupt HER2 dimerization and subsequent downstream signalling events leading to apoptosis of cancer cells. The phase transformation of peptides enables specific HER2 targeting, and inhibition of HER2 dimerization blocks the expression of proliferation and survival genes in the nucleus. We demonstrate, in mouse xenograft models, that these transformable peptides can be used as a monotherapy in the treatment of HER2⁺ breast cancer.

Human epidermal growth factor receptor 2 (HER2) is overexpressed in >20% of breast cancers and, to a lesser degree, in gastric, colorectal, ovarian and bladder cancers^{1–5}. Unlike those cancers caused by mutated or fusion oncogenes (for example, epidermal growth factor receptor (EGFR) in lung cancers) that respond well to monotherapy^{6,7}, cancers with HER2 overexpression often require drug combinations^{8,9}. This occurs because this group of tumours are driven by gene amplification and massive overexpression of HER2. HER2 is a receptor tyrosine kinase that is normally activated via induced dimerization with itself or with its family members EGFR, HER3 or HER4 (refs. 10–12). In HER2⁺ tumours, HER2s are massively overexpressed and constitutively dimerized leading to unrelenting activation of downstream proliferation and survival pathways and malignant phenotype. Here, we report on a HER2-mediated, peptide-based, non-toxic transformable nanoparticle that is highly efficacious as a monotherapy against HER2⁺ breast cancer xenograft models.

Supramolecular chemistry involves chemical systems formed by self-assembly of molecular subunits via non-covalent interactions^{13–16}. Harnessing the advantages of the dynamic nature and adaptive behaviour of supramolecular chemistry, Xu et al. and Wang et al. proposed an ‘in vivo self-assembly’ strategy for in situ construction of nanomaterials in vivo^{17–21}. Here, we designed and synthesized a smart supramolecular peptide, BP-FFVLK-YCDGFYACYMDV, capable of (1) assembling into nanoparticles (NPs) under aqueous conditions and in the circulation, and (2) in situ transformation into a nanofibrillar (NF) structure on binding to the cell surface HER2 at tumour sites. This transformable peptide monomer (TPM) is comprised of three discrete functional domains: (1) the bis-pyrene (BP) moiety with aggregation-induced emission (AIE) property for fluorescence reporting, and as a hydrophobic core to induce the formation of micellar NPs; (2) FFVLK, reverse sequence of the KLVFF β -sheet-forming peptide domain derived from β -amyloid (A β)

peptide^{22–24}; and (3) the YCDGFYACYMDV disulfide cyclic peptide HER2-binding domain^{25–27}, an anti-HER2/neu antibody peptidic mimic derived from the primary sequence of the CDR-H3 loop of the anti-HER2 rhuAb 4D5. Under aqueous conditions, TPM will self-assemble into spherical NPs in which the BP and FFVLK domains constitute the hydrophobic core and YCDGFYACYMDV peptide constitutes the negatively charged hydrophilic corona. NPs, injected intravenously (IV) into mice bearing HER2⁺ tumours, were found to be preferentially accumulated at the tumour site. Following interaction with HER2 on the tumour cell surface, the NPs underwent in situ transformation into a fibrillar structural network which, in turn, suppressed the dimerization of HER2 and prevented downstream cell signalling and the expression of proliferation and survival genes in the nucleus (Fig. 1). These structural transformation-based supramolecular peptides represent a class of receptor-mediated targeted nanotherapeutics against cancers.

Self-assembly and fibrillar transformation

The transformable peptide monomer1 (TPM1, BP-FFVLK-YCDGFYACYMDV) and the negative control peptides TPM2 (BP-GGAAK-YCDGFYACYMDV), TPM3 (BP-FFVLK-PEG₁₀₀₀) and TPM4 (BP-GGAAK-PEG₁₀₀₀) were synthesized and characterized (Fig. 2a, Table 1 and Supplementary Figs. 1 and 2). As the proportion of water in the mixed solvent (water and DMSO) of the TPM1 solution was increased, there was a gradual decrease in absorption peaks (250–450 nm) reflecting the gradual formation of NPs1 via self-assembly (Fig. 2b). Concomitantly, the fluorescence peak at 520 nm was found to increase dramatically due to the AIE fluorescence properties of BP dye (Fig. 2c)^{28,29}. TPM2, TPM3 and TPM4 all showed similar self-assembling properties (Supplementary Fig. 3a). NPs1–4 were analysed by dynamic light scattering (DLS) and transmission electron microscopy (TEM) (Fig. 2d and Supplementary Fig. 3b). The diameters of NPs1–4 were found to be around 20, 30,

¹Department of Biochemistry and Molecular Medicine, UC Davis NCI-designated Comprehensive Cancer Center, University of California Davis, Sacramento, CA, USA. ²Department of Radiation Oncology, School of Medicine, University of California Davis, Sacramento, CA, USA. ³Department of Oncology, Xiangya Hospital, Central South University, Hunan, China. ⁴CAS Center for Excellence in Nanoscience, CAS Key Laboratory for Biomedical Effects of Nanomaterials and Nanosafety, National Center for Nanoscience and Technology, Beijing, China. ⁵Division of Hematology and Oncology, Department of Internal Medicine, School of Medicine, University of California Davis, Sacramento, CA, USA. ⁶These authors contributed equally: L. Zhang, D. Jing. *e-mail: wanglei@nanocr.cn; kslam@ucdavis.edu

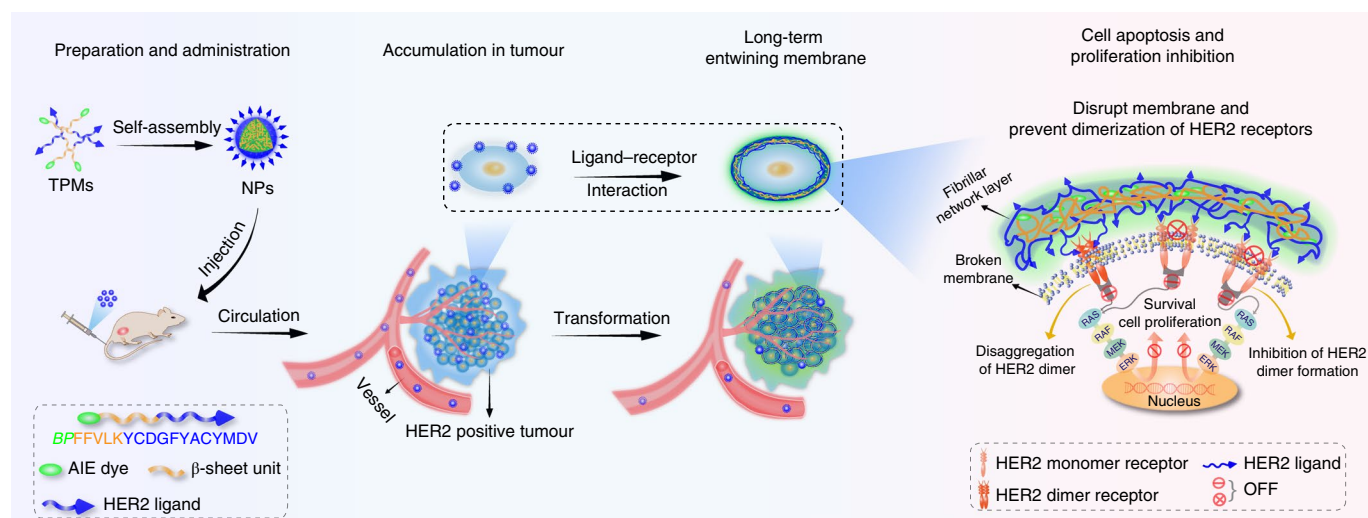


Fig. 1 | Transformable peptide nanoparticles can arrest HER2 signalling. Schematic illustration of self-assembly, accumulation and in situ fibrillar transformation of TPMs in tumour tissue of HER2⁺ cancer, followed by extracellular and intracellular pro-apoptotic and anti-proliferative events.

25–60 and 20 nm, respectively. The critical aggregation concentration (CAC) of NPs1–4 was calculated as 4.2, 7.0, 10.5 and 9.8 μ M, respectively (Supplementary Fig. 3c).

The soluble extracellular domain of HER2 protein was used to investigate the interaction of HER2 with NPs1 *in vitro*. The minimum ratio of HER2 protein/peptide ligand required for maximum promotion of fibrillar network formation was determined to be 1/1,000 (Supplementary Fig. 4). NPs1 was found to maintain a spherical structure at around 20 nm before interaction with HER2 (Fig. 2d). After incubation at room temperature with HER2 protein for 30 min, a small number of particulate nanofibrillar structures (NFs1, width diameter \sim 9 nm) became apparent; more NFs1 were detected at 6 h. By 24 h, a fibrillar network with a wide size distribution was clearly detectable. No transformation was observed in NPs1 preparation without the addition of HER2 protein, even after 24 h (Supplementary Fig. 5). The structural transformation from NPs1 to NFs1 was also confirmed in solution by DLS (Fig. 2e). In contrast, similar treatment of NPs2–4 with HER2 revealed no significant changes over 24 h (Supplementary Fig. 6). Common features of the TPMs that formed these three negative control NPs included the lack of concurrent presence of the two essential domains for receptor-mediated transformation in NPs1: HER2 ligand and KLVFF β -sheet-forming peptide. Circular dichroism spectroscopy analysis of the transformation process showed a gradual progression of the negative signal at 216 nm and positive signal at 195 nm, and therefore β -sheet formation over 24 h (Fig. 1f)^{22,30}. No obvious change in circular dichroism signal was observed in NPs2–4 (Supplementary Fig. 7). The unique AIE fluorescent property of BP was used to monitor the kinetics of TPM1 transformation (Fig. 2g). The fluorescence intensity of BP in NPs1 fell by \sim 11.8% after the addition of HER2 for 30 min, but increased as transformation to NFs1 progressed and eventually reached \sim 61.7% by 24 h. A more detailed study and interpretation of this phenomenon is shown in Supplementary Fig. 8a,b. The zeta potential of NPs1 was found to change from -12 to -30 mV over time during the transformation process (Supplementary Fig. 8c,d). The serum and proteolytic stability of NPs over 7 d at 37 $^{\circ}$ C was good (Supplementary Fig. 8e–l).

Morphological characterization on cell surface

Six hours after incubation of HER2⁺ breast cancer cell lines (SKBR-3 and BT474 cells) with NPs1, a strong green fluorescence signal was observed on the cell surface but not within the cells (Fig. 3a,b). In contrast, for MCF-7 breast cancer cells with a low expression level

of HER2, the majority of the fluorescent signal was found within the cells after 6–24 h (Fig. 3c and Supplementary Fig. 9), indicating that cell surface display of HER2 protein was required for the transformation of NPs1 to the nanofibrillar network in the vicinity of the cell. Cellular uptake of NPs1 by MCF-7 cells was found to be inhibited by amiloride (2 mM), β -CD (5 mM) and hypertonic sucrose (450 mM), indicating that NPs1 might have entered the cell by caveolae-, clathrin- or macropinocytosis-dependent endocytosis (Supplementary Figs. 10 and 11).

Radiotherapy is commonly used in the management of breast cancer patients³¹. It has previously been reported that long-term fraction ionizing radiation can induce HER2 expression, both clinically and in experimental models^{32,33}. In fact, the HER2⁺ MCF-7/C6 tumour cell line used in our current study was derived from a HER2⁻ human breast cancer MCF-7 cell line that had undergone 30 d of fraction ionizing radiation induction, followed by colony formation and clonal isolation (Supplementary Fig. 12)^{32,34}. MCF-7/C6 cells, with fivefold higher HER2 than parent MCF-7 cells (Fig. 3d), exhibit the characteristics of radiation resistance, more aggressive phenotype and enhanced levels of cancer stem cell properties. After 30-min incubation of MCF-7/C6 cells with NPs1 (50 μ M), green fluorescent dots were observed on the cell membrane (Fig. 3e). By 24 h, a luxuriant green fluorescent layer was found surrounding the entire cell.

To further validate the binding of NPs1 to HER2, we used anti-HER2 (29D8) monoclonal antibody followed by fluorescent red secondary antibody to detect HER2 on MCF-7/C6 cells. Overlapping green fluorescence (BP) with red fluorescence (HER2) was found around the periphery of the two adjoined cells except at the adhesion interface, which was not accessible to NPs1 present in the culture medium (Fig. 3f). Three-dimensional image rendering of these two cells is shown in Supplementary Fig. 13. The cellular distribution of negative control NPs (NPs2–4) was also investigated in MCF-7/C6 cells. After 24-h incubation, the majority of the fluorescent signal was found within the cells rather than on the cell surface, with most of the internalized nanoparticles degraded in lysosomes (Supplementary Figs. 14–17). Scanning electron microscopy (SEM) confirmed the presence of a nanofibrillar network on the surface of NPs1-treated MCF-7/C6 cells (Fig. 3g). In contrast, no nanofibrillar structure was detected on the surface of untreated cells or those treated with NPs2–4 (Supplementary Fig. 18). TEM showed similar results, with abundant bundles of nanofibrils detected on the surface of, and between, MCF-7/C6 cells after incubation

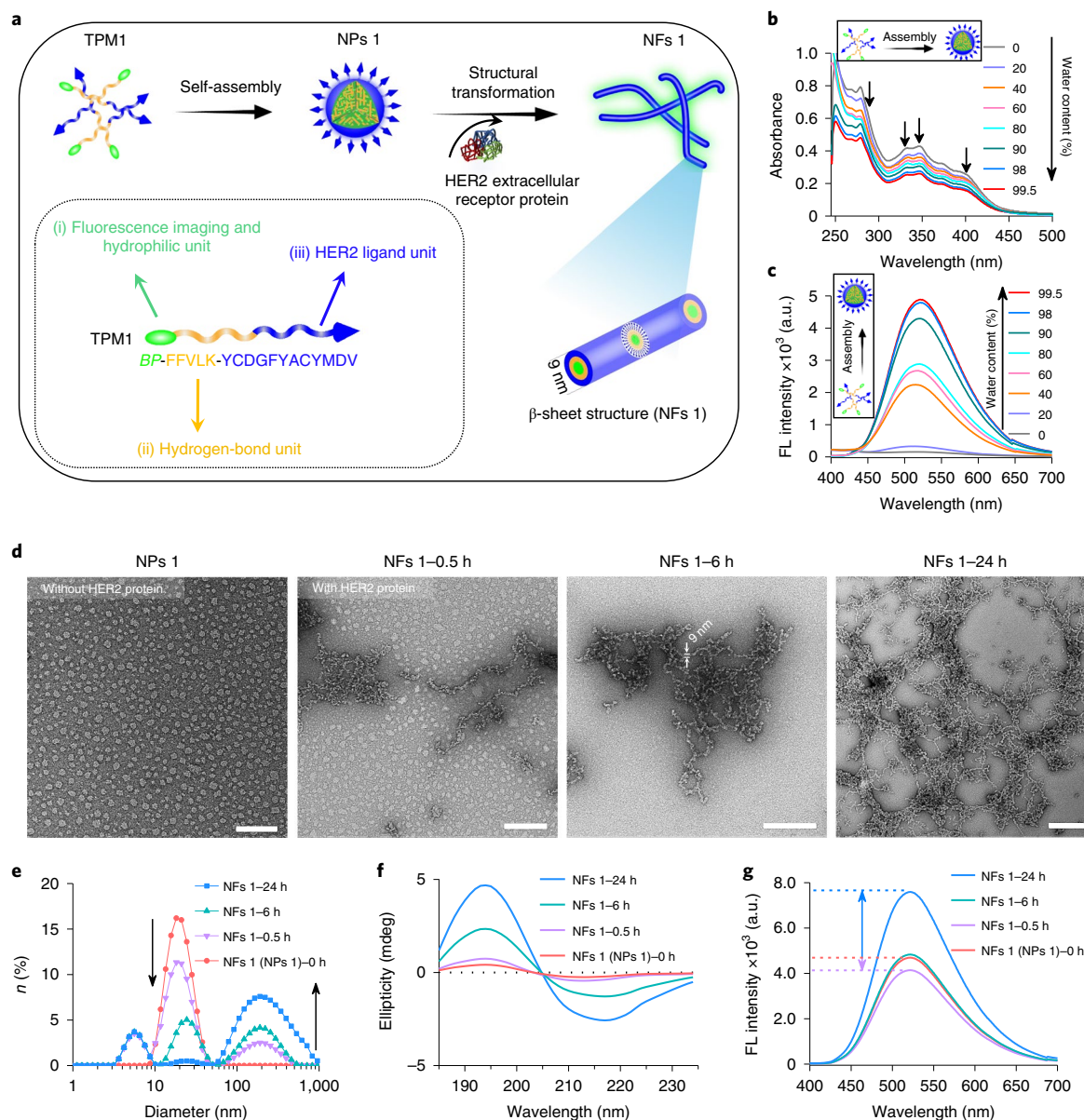


Fig. 2 | Assembly and fibrillar transformation of transformable TPM1 BP-FFVLK-YCDGFYACYMDV. **a**, Schematic illustration of self-assembly and in situ structural transformation of TPM1. **b,c**, Changes in UV-vis absorption (**b**) and fluorescence (FL) of NPs1 (**c**) following the gradual addition of water (from 0 to 99.5%) to a solution of NPs1 in DMSO; excitation wavelength, 380 nm; experiments were repeated three times. **d**, TEM images of initial NPs1 and NPs1 transformed into nanofibres (NFs1) after interaction with HER2 protein ($M_w \approx 72$ kDa) at different time points (0.5, 6 and 24 h). Scale bars, 100 nm. Experiments were repeated three times. **e-g**, Variation in size distribution (**e**), circular dichroism spectra (**f**) and fluorescence signal (**g**) of initial NPs1 and NFs1 at different time points. A representative image from three independent tests is shown. The molar ratio of HER2 protein/peptide ligand was approximately 1/1,000. a.u., arbitrary units; mdeg, millidegrees.

Table 1 | Molecular composition of TPM1-4

TPM	BP	FFVLK	GGAAK	YCDGFYACYMDV	PEG ₁₀₀₀
1	+	+	-	+	-
2	+	-	+	+	-
3	+	+	-	-	+
4	+	-	+	-	+

TPM1: BP-FFVLK-YCDGFYACYMDV (with HER2-binding peptide and β -sheet-forming peptide). TPM2: BP-GGAAK-YCDGFYACYMDV (with HER2-binding peptide but without β -sheet-forming peptide). TPM3: BP-FFVLK-PEG₁₀₀₀ (without HER2-binding peptide but with β -sheet-forming peptide). TPM4: BP-GGAAK-PEG₁₀₀₀ (with neither HER2-binding peptide nor β -sheet-forming peptide).

with NPs1 for 24 h (Fig. 3h). The presence of fibrillar structures formed further away from the cell surface was determined to have been induced by tumour cell-secreted exosomes displaying HER2 (Supplementary Fig. 19). No nanofibrillar structure was detected on untreated MCF-7/C6 cells or those treated with the three negative control NPs for 24 h. A minimal number of nanofibrils was detected on the surface of NPs1-treated MCF-7 cells with low HER2 levels (Supplementary Fig. 20).

In vitro extracellular and intracellular mechanisms

It has recently been reported that nanofibrils self-assembled from carbohydrate or peptide amphiphiles on cell membranes could alter cell fate³⁵⁻³⁹. It is conceivable that HER2-mediated transformation of

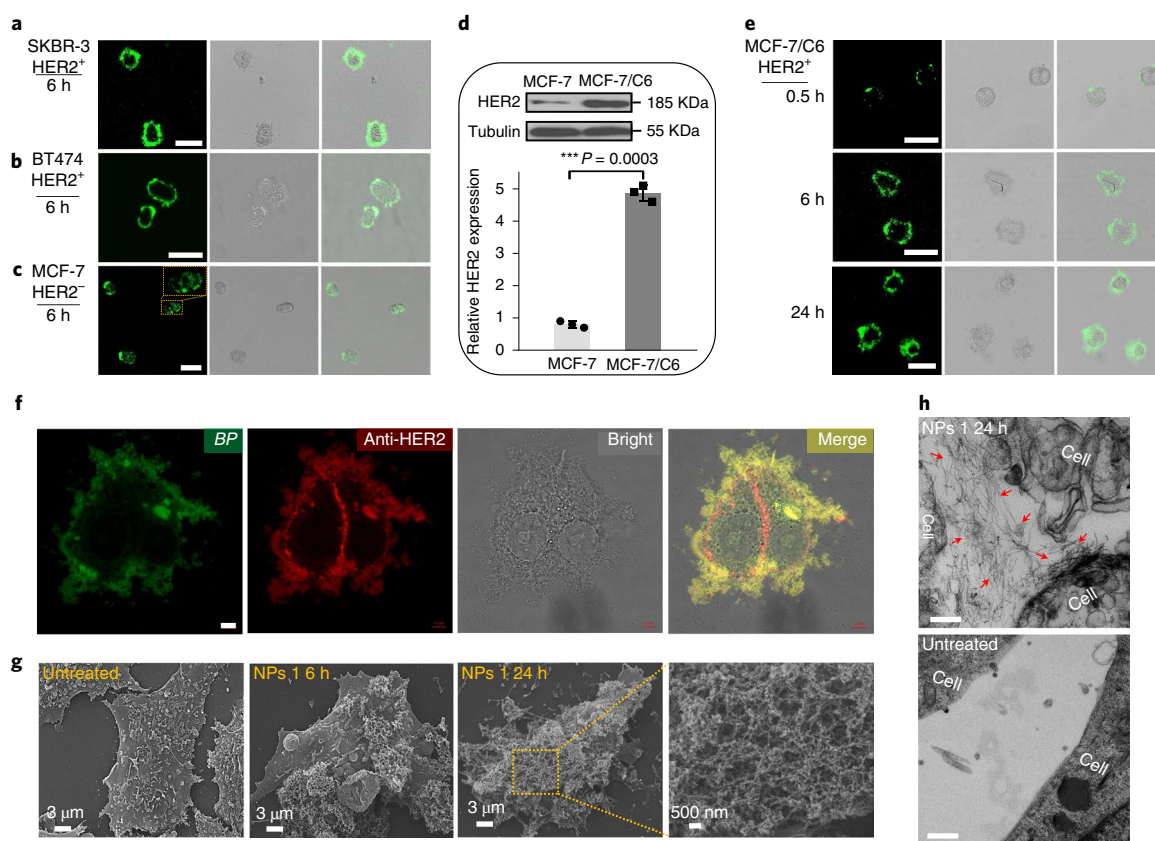


Fig. 3 | Morphological characterization of fibrillar-transformable NPs1 incubation with cultured HER2⁺ cancer cells. **a–c**, Cellular fluorescence distribution images of NPs1 interaction for 6 h with SKBR-3 cells (HER2⁺) (**a**), BT474 cells (HER2⁺) (**b**) and MCF-7 cells (HER2⁻) (**c**). Scale bars, 50 μ m. Experiments were repeated three times. **d**, Immunoblot and quantitative analysis of relative HER2 protein expression in MCF-7 and MCF-7/C6 cells. Data are presented as mean \pm s.d., $n = 3$ independent experiments. *** $P < 0.001$ (two-tailed Student's *t*-test). Representative image from three independent tests is shown. **e**, Cellular fluorescence distribution images of NPs1 interaction with MCF-7/C6 cells (HER2⁺) at different time points (0.5, 6 and 24 h). Scale bar, 50 μ m. Experiments were repeated three times. **f**, Fluorescence binding distribution images of the nanofibrillar network of NPs1 and HER2 antibody (29D8 rabbit Ab and HER2 peptide of NPs1 recognize different epitopes of HER2 receptor) on the cell membrane of MCF-7/C6 cells. HER2 antibody was used to label HER2 receptors. Scale bar, 5 μ m. Experiments were repeated three times. **g**, SEM images of untreated MCF-7/C6 cells and cells treated with NPs1 for 6 and 24 h. Experiments were repeated three times. **h**, TEM images of untreated MCF-7/C6 cells and cells treated with NPs1 for 24 h. Red arrows indicate the fibrillar network. Scale bars, 200 nm. Experiments were repeated three times. The concentration of NPs1 was 50 μ M.

nanoparticles to a nanofibrillar network could impair HER2 dimerization, leading to suppression of downstream signal transduction. To demonstrate this plausible mechanism, we first incubated MCF-7/C6 cells with NPs1, NPs2 or phosphate buffered saline (PBS) for 8 h (Fig. 4a). As expected, NPs1 induced thick nanofibrillar network formation (fluorescent green) around the cell surface, whereas negative control NPs2 generated only a scant fluorescent green signal.

The cytotoxic effect of NPs1 and the three negative control NPs on MCF-7/C6 cells after 48 h incubation was determined by MTS assay. Treatment with NPs1 resulted in significant cell death in a dose-dependent manner (Fig. 4b). Similar results were obtained for two other HER2⁺ breast cancer cell lines, SKBR-3 and BT474 (Supplementary Fig. 21a,b). However, when MCF-7 cells with low HER2 levels were treated with these four NPs, no obvious cytotoxicity was observed even at the highest concentration of 300 μ M (Supplementary Fig. 21c). Treatment of MCF-7/C6 cells with NPs1 resulted in downregulation of anti-apoptotic protein Bcl-2 and upregulation of apoptotic protein Bax, in a dose-dependent manner (Fig. 4c). To study the effect of NPs1 on HER2 dimerization, we employed a simple method of brief chemical cross-linking with 0.01% glutaraldehyde followed by immunoblot analysis with anti-HER2 antibody⁴⁰. This allowed us to determine the relative level of

cellular HER2 dimers and monomers. It is clear from Fig. 4d,e that NPs1 was able to inhibit HER2 dimerization in a dose- and time-dependent manner, indicating that, not only could it inhibit HER2 dimerization, but it could also promote the conversion of HER2 from dimers to monomers. In addition, the MAPK pathway was suppressed in a dose-dependent manner with a significant decrease in phosphorylation levels of Erk, Mek and Raf-1 over time (Fig. 4f). For the purposes of comparison, MCF-7/C6 cells were incubated with 50 μ M of each NPs for 36 h, and Herceptin was used as a positive control (Fig. 4g). Like Herceptin, NPs1 strongly inhibited pErk, pMek and pRaf-1. In contrast, the three negative control NPs did not significantly alter the phosphorylation level of Erk, Mek and Raf-1. Together, these data strongly support our notion that transformation of NPs1 to a nanofibrillar network on the surface of HER2⁺ tumour cells results in inhibition of HER2 dimerization and conversion of HER2 dimers to monomers, leading to inhibition of downstream proliferation and survival cell signalling, and cell death.

In vivo evaluation of fibrillar-transformable nanoparticles

NPs1 was found to be non-toxic: blood counts, platelets, creatinine and liver function tests obtained from normal Balb/c mice treated with eight consecutive q.o.d. doses of NPs1 were within normal limits (Supplementary Figs. 22 and 23). In vivo blood

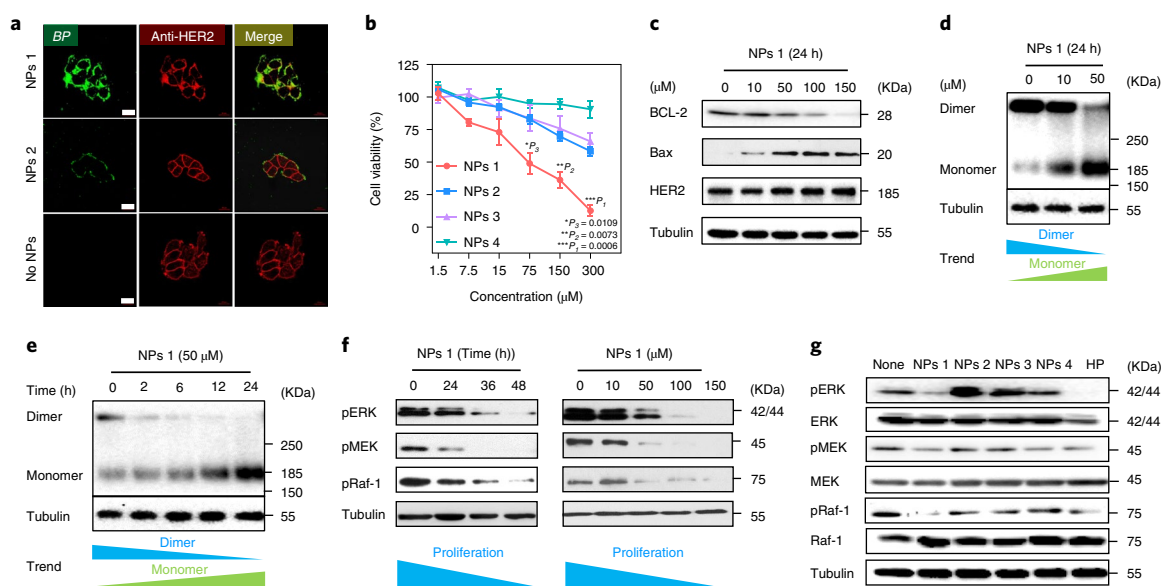


Fig. 4 | Extracellular and intracellular mechanisms of fibrillar-transformable nanoparticle interaction with MCF-7/C6 breast cancer cells. **a**, Fluorescence binding distribution images of NPs1 and NPs2 binding HER2 receptors of MCF-7/C6 cells for 8 h. HER2 antibody (29D8 rabbit Ab and HER2 peptide of NPs1 and NPs2 recognize different epitopes of HER2 receptor) was used to label HER2 receptors. The concentration of NPs1 and NPs2 was 50 μM. Scale bar, 20 μm. Experiments were repeated three times. **b**, Viability of MCF-7/C6 cells after incubation with NPs1-4 at different concentrations for 48 h. Data are presented as mean ± s.d., $n = 3$ independent experiments. Statistical significance was calculated by ANOVA with a Tukey post hoc test. * $P < 0.05$, ** $P < 0.01$, *** $P < 0.001$. **c**, Immunoblot analysis of apoptosis-related proteins and HER2 total protein in MCF-7/C6 cells treated by NPs1 for 24 h at different concentrations. Experiments were repeated three times. **d, e**, Immunoblot analysis of inhibition and disaggregation mechanism of HER2 protein dimer in MCF-7/C6 cells treated by NPs1 for 24 h at different concentrations (**d**) and with 50 μM at different time points (**e**). Experiments were repeated three times. **f**, Immunoblot analysis of inhibition mechanism of proliferation protein in MCF-7/C6 cells treated by NPs1 at 50 μM at different time points and at 24 h under different concentrations. Experiments were repeated three times. **g**, Immunoblot analysis of the inhibition mechanism of proliferation protein in MCF-7/C6 cells treated by NPs1-4 and Herceptin (HP) at 36 h. The concentration of NPs1-4 was 50 μM and that of HP, as a positive control group, was 15 μg ml⁻¹. Experiments were repeated three times.

pharmacokinetic studies indicated that NPs1 possessed a long circulation time (Supplementary Fig. 24). For biodistribution studies, mice bearing the MCF-7/C6 tumour were administered IV NPs1; 10, 24, 48, 72 and 168 h later, tumour and main organs were collected for ex vivo fluorescent imaging (Fig. 5a,b and Supplementary Fig. 25). Fluorescent signal persisted in tumour tissue for >3 d, with significant residual signal present even after 7 d. In contrast, fluorescent signal in normal organs began to decline after 10 h and was almost undetectable in the main organs at 72 h, while histological examination of excised normal organs revealed no pathology (Supplementary Figs. 26 and 27). Fluorescent micrography of tumour and overlying skin revealed intense fluorescent signal in tumour but negligible signal in normal skin (Fig. 5c). As shown in Supplementary Fig. 28, the green fluorescence signal from BP was found throughout the entire tumour tissue section, not only at the periphery. In vivo biodistribution studies on NPs2-4 were also performed in the same tumour model (Supplementary Fig. 29). At 72 h, fluorescent signal in tumour derived from mice treated with NPs1 was found to be two- to threefold higher than that of mice treated with NPs2-4 (Fig. 5d,e). Prolonged retention of fluorescent signal in NPs1-treated mice, even after 7 d, could be attributed to in situ receptor-mediated transformation of NPs1 into NFs1 networks in the tumour micro-environment. TEM studies on excised tumour sections, 72 h after IV administration, showed abundant bundles of nanofibrils in the extracellular matrix while no such nanofibrils were observed in negative control NP-treated and untreated mice (Fig. 5f). In addition, many cells in tumour tissue excised from NPs1-treated mice appeared to be dying, with large intercellular spaces. The TEM images of organs excised from the same

mouse were found to be normal, with no presence of nanofibrillar networks (Supplementary Fig. 30).

Therapeutic efficacy studies of NPs1-4 were performed in MCF-7/C6 HER2⁺ breast cancer-bearing mice (Fig. 6a). NPs were injected consecutively eight times q.o.d. in the tail vein and observed continuously for 40 d. Tumour volume of NPs1-treated mice gradually shrank and was totally eliminated after treatment, with no sign of recurrence (Fig. 6b and Supplementary Fig. 31). In contrast, none of the other three negative control groups elicited any significant tumour response. No significant side effects were observed in this study (Fig. 6c). The survival curves correlated well with tumour growth results (Fig. 6d). In contrast, all mice in the PBS-, NPs2-, NPs3- and NPs4-treated groups died, within 51, 63, 57 and 60 d, respectively.

To better understand the in vivo anti-tumour mechanism of NPs1, mice were sacrificed and residual tumours collected for biochemical and morphological assessment after three consecutive q.o.d. injections of NPs1 (Fig. 6e). The degree of cell kill was found to correlate well with that of fluorescent intensity: necrosis was detected in those tumour areas with strong fluorescence intensity (Fig. 6f). To understand how the nanofibrillar network kills HER2⁺ tumour cells, we performed high-magnification TEM on tumours obtained from NPs1-treated mice. The TEM image of necrotic or necroptotic cells (Fig. 6g) revealed that the plasma membrane was ruptured, with abundant fibrillar nanostructures present within the ruptured cell; some nanofibrillar bundles were found adjacent to the nuclear envelope of the nucleus. No significant cell kill was detected in tumour sections obtained from mice treated with PBS, NPs2, NPs3 or NPs4 (Supplementary Fig. 32). The expression level of Ki-67 in tumour tissue was found to be markedly reduced

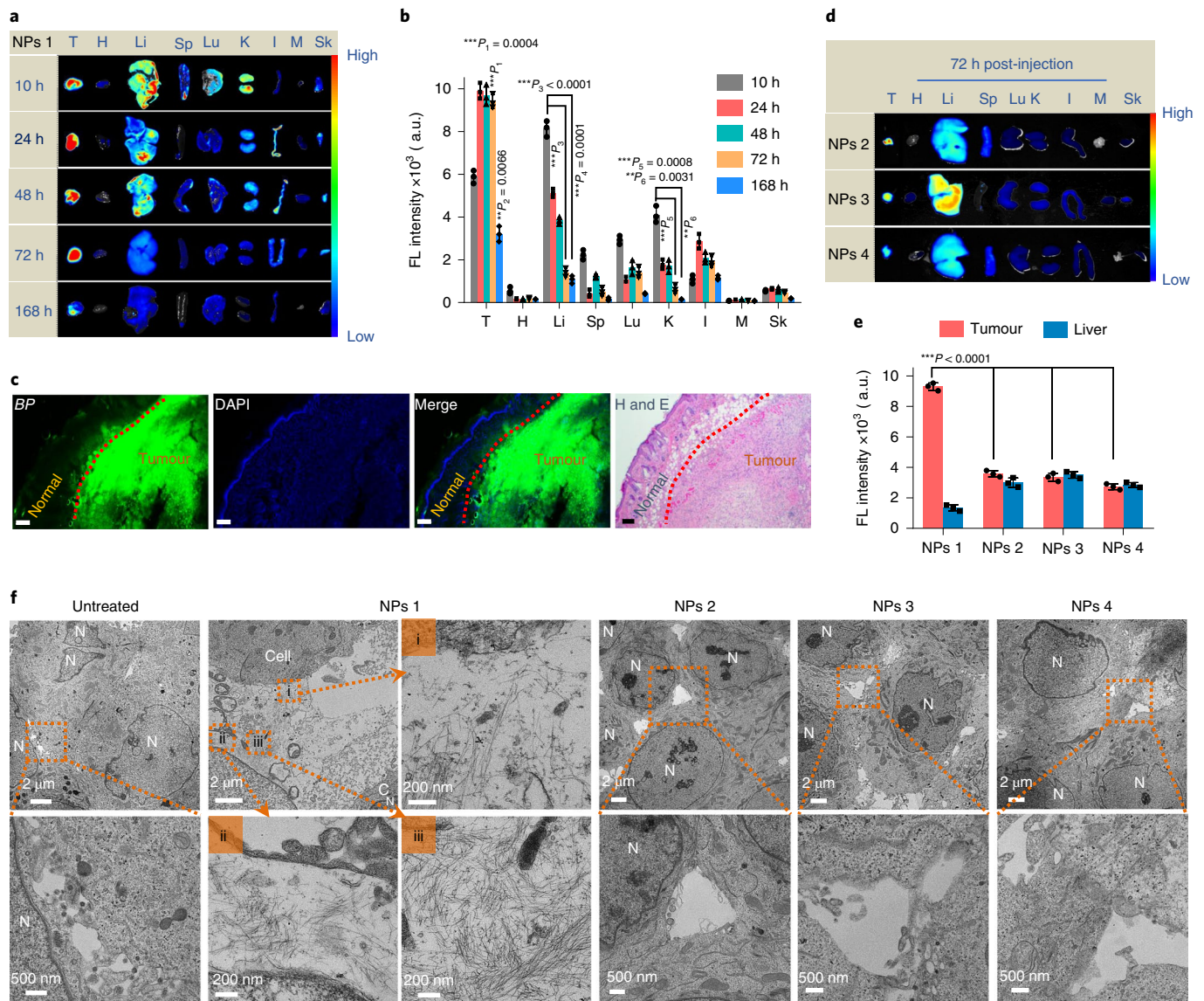


Fig. 5 | In vivo evaluation of fibrillar-transformable nanoparticles. **a, b**, Time-dependent ex vivo fluorescence (FL) images (**a**) and quantitative analysis (**b**) of tumour tissues and major organs (heart (H), liver (Li), spleen (Sp), lung (Lu), kidney (K), intestine (I), muscle (M) and skin (Sk)) collected at 10, 24, 48, 72 and 168 h post-injection of NPs1. Data are presented as mean \pm s.d., $n=3$ independent experiments. Statistical significance was calculated by one-way ANOVA with a Tukey post hoc test; $**P < 0.01$, $***P < 0.001$. Fluorescence signal in tumour tissue at 72 and 168 h compared with other organs displays tumour accumulation and in situ transformation of the fibrillar network with extended retention time; the fluorescence signal in liver and kidney at 10 h compared with that at 72 and 168 h shows that NPs1 could rapidly be removed. **c**, Fluorescence distribution images and H&E image of NPs1 in tumour tissue and normal skin tissue at 72 h post-injection (green, BP of NPs1; blue, DAPI; scale bars, 100 μ m). Experiments were repeated three times. **d**, Time-dependent ex vivo fluorescence images of tumour tissues and major organs collected 72 h post-injection of NPs2-4. **e**, Quantitative analysis of tumour and liver tissues collected 72 h post-injection of NPs1-4. Data presented as mean \pm s.d., $n=3$ independent experiments, $***P < 0.001$. The fluorescence signal of tumour tissue in the NPs1 group compared with that in other control groups shows that fibrillar networks in the former promoted extended retention time at the tumour site. **f**, TEM images of distribution in tumour tissue and in situ fibrillar transformation of NPs1-4 at 72 h post-injection, and of the untreated group. The dose of NPs1-4 per injection was 8 mg kg⁻¹. N, nucleus. Experiments were repeated three times. Statistical significance was calculated by one-way ANOVA with a Tukey post hoc test. a.u., arbitrary units.

compared to tumour obtained from mice treated with negative control NPs (Fig. 6h).

Tumours from NPs1-treated mice were excised for biochemical studies (Fig. 6i). The total HER2 level of tumour cells remained unchanged, but phosphorylation of Erk, Mek and Raf-1 was found to be markedly reduced compared to the other negative control groups. Together, the data clearly demonstrated that NPs1 was highly effective in suppressing downstream proliferative and survival cell signalling at the tumour tissue level. We also found that

the cell surface fibrillary network markedly impaired the cellular uptake of hydrophilic Rhodamine 6 G dye (Supplementary Fig. 33), suggesting that tumour cell death may have been caused in part by impaired uptake of vitamins and nutrients. To better investigate the universality of NPs1 as an efficacious therapeutic against HER2⁺ tumours, two other human HER2⁺ breast cancer xenograft models (BT474 and SKBR-3) were chosen for our studies. As shown in Fig. 6j and Supplementary Fig. 34a, the tumour volume in mice treated with NPs1 responded very well, with almost complete elimination

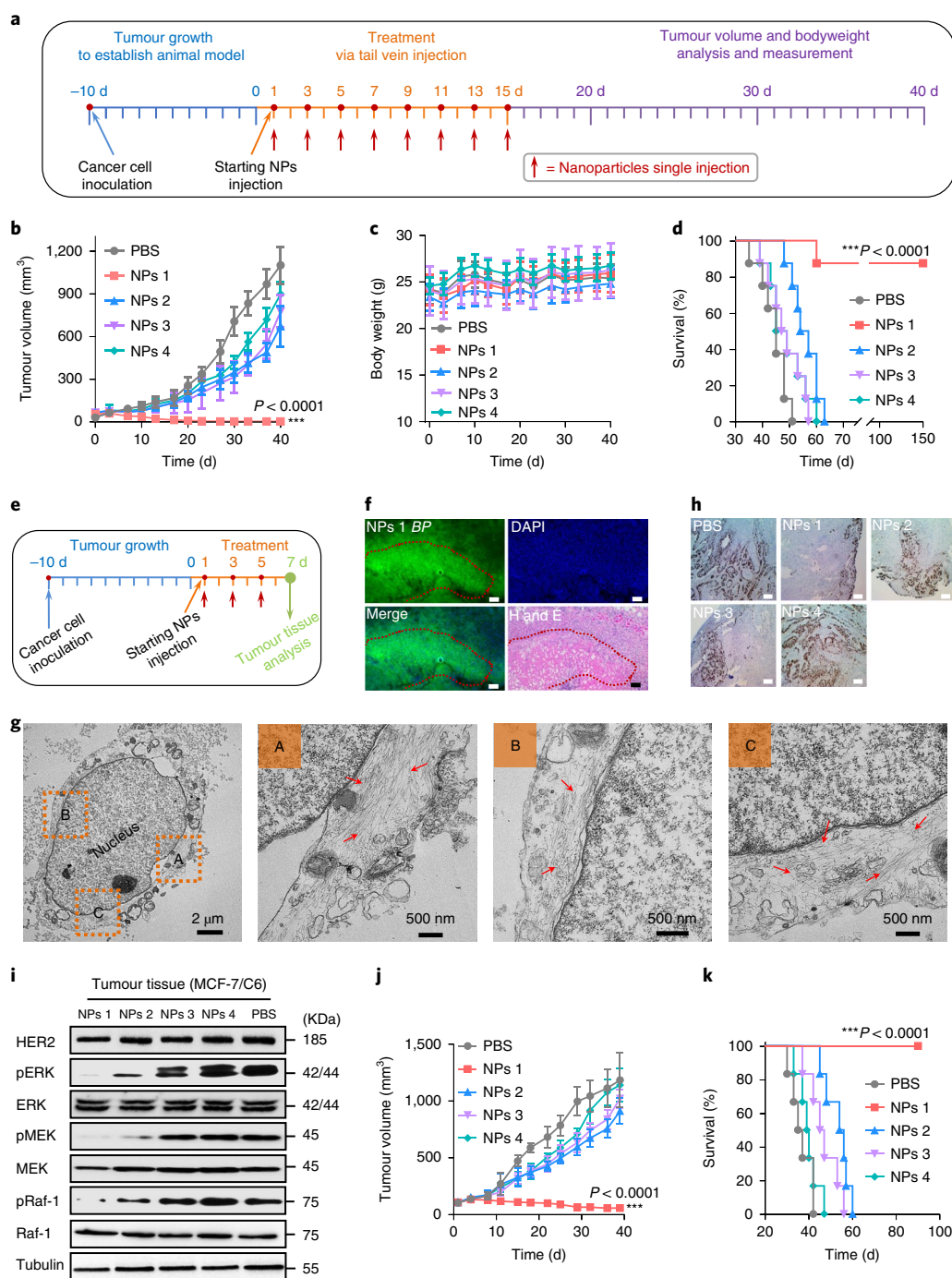


Fig. 6 | Anti-tumour activity of fibrillar-transformable nanoparticles in Balb/c nude mice bearing HER2⁺ breast tumour. **a**, Schematic illustration of tumour inoculation and treatment protocol for mice. **b,c**, Observation of tumour inhibitory effect (**b**) and weight change (**c**) of mice in subcutaneous tumour model over 40 d of treatment ($n=8$ per group; the dose of NPs1–4 was 8 mg kg^{-1} per injection). Data are presented as mean \pm s.d. $***P < 0.001$. **d**, Cumulative survival of different treatment groups of mice bearing MCF-7/C6 breast tumour. Seven of the eight mice receiving NPs1 treatment survived >150 d with no sign of tumour recurrence. One of the eight mice, no longer with detectable tumour, died at around d 60 for reasons unknown. **e**, Schematic illustration of three-times treatment protocol of mice for tumour tissue analysis ($n=6$ per group; NPs1–4 dose as in **b,c**). **f**, Fluorescence distribution images in tumour tissue and H&E anti-tumour image after three injections of NPs1 (green, BP of NPs1; blue, DAPI; scale bars, 100 μ m). Experiments were repeated six times; a representative image is shown. **g**, Representative TEM images of late membrane rupture and cell death by the nanofibrillar network after three injections of NPs1; red arrows indicate fibrillar network. **h**, Ki-67 staining images of tumour tissues treated by the different groups after three doses of treatment; scale bars, 25 μ m. Experiments were repeated six times; a representative image is shown. **i**, Immunoblot analysis of the inhibition mechanism of HER2 protein and proliferation proteins in MCF-7/C6 tumour tissues treated by the five different groups after three doses of treatment. Experiments were repeated six times; a representative image is shown. **j**, Observation of tumour inhibitory effect in subcutaneous BT474 HER2⁺ breast cancer models over 40 d of treatment ($n=6$ per group; NPs1–4 dose as in **a**). Data are presented as mean \pm s.d. $***P < 0.001$ compared with PBS control group. **k**, Cumulative survival rates of different treatment groups of mice bearing BT474 breast tumours. Statistical significance was calculated by one-way ANOVA with a Tukey post hoc test.

of BT474 and complete elimination of SKBR-3 by d40, again with no significant side effects (Supplementary Fig. 34b,c). Survival curves of the NPs1-treated group in the BT474 model correlated well with tumour growth results (Fig. 6k).

One known side effect of Herceptin is cardiotoxicity^{31,41}, and therefore it cannot be administered together with cardiotoxic drugs such as doxorubicin⁴². We found that NPs1 was able to undergo fibrillar transformation, not only when interacting with human HER2 but also with murine HER2 expressed on murine breast cancer cells (4T1/HER2) (Supplementary Fig. 35). Thus far we observed no cardiotoxic effects in our xenograft studies with NPs1; no uptake of NPs1 in the myocardium was detected. This is not surprising, since the coronary vessels were expected to be intact and the 20-nm NPs1 would not have been able to reach the myocardium. The fact that NPs1 was highly efficacious against three different HER2⁺ tumours warrants further preclinical and clinical development of NPs1 against HER2⁺ breast, ovarian, gastric and bladder cancers. There is good clinical evidence that certain, originally HER2⁻, breast cancers can be induced to express HER2 after long-term fraction ionizing radiation³². This further extends the patient population that might benefit from this HER2-mediated transformable nanoplatform.

When compared with current anti-HER2 therapy, NPs1 at 50 μ M displayed similar inhibitory effects on downstream proliferation and survival cell signalling to that of combination trastuzumab and pertuzumab (Supplementary Fig. 36a–c). We believe that combination therapy of NPs1 with pertuzumab could be synergistic, because the former has been shown to downregulate HER2 homodimers and the latter is known to downregulate HER2 heterodimers. Another promising combination therapy is NPs1 plus lapatinib. Our *in vitro* data clearly demonstrated that such a drug combination could suppress HER2 dimerization and downregulate the expression of downstream proliferation genes and increase in cytotoxicity (Supplementary Fig. 36d–h). Receptor-mediated therapeutic fibrillar transformation is not limited to HER2-binding ligands against HER2⁺ cancer. Our most recent data indicate that the concept is general and can be applied to other cancer cell surface receptors, including $\alpha_5\beta_1$ integrin, which is overexpressed in many epithelial cancers⁴³. Transformable nanoparticles decorated with LXY30 (ligand against $\alpha_5\beta_1$ integrin) were found capable of undergoing *in situ* fibrillar transformation both in cell culture and *in vivo* at the tumour site.

Data derived from both TEM and DLS clearly demonstrated that the transformation process from NPs1 to NFs1 did not occur in bulk and instantaneously but, rather, gradual recruitment occurred over a 24-h period (Fig. 2d). Assuming that the total volume of the nanostructure did not change significantly during the transformation process, the surface area of each nanostructure, from 20-nm micelle to 9-nm-diameter fibril, is calculated to have increased by about 58%. Such increase in surface area would allow (1) interaction of 58% more HER2 receptors with the nanofibril structure and (2) denser KLVFF β -sheet packing along the long axis of the nanofibril, resulting in a thermodynamically more stable structure. We believe these could be the two driving forces for nanotransformation. How this might occur at the molecular level is not clear at the present time. What we did observe was that there was a slight initial decrease in fluorescence of NPs1 in the first 40 min, followed by a gradual increase in fluorescence as transformation to NFs1 occurred over time, reflecting changes in conformation and packing of the TPMs within the nanostructure when exposed to HER2 (Supplementary Fig. 8a).

Conclusions

In this study we have demonstrated that NPs1 *per se* as a monotherapy is non-toxic and efficacious in curing a large percentage of mice bearing HER2⁺ breast cancer xenografts. Replacement of HER2-binding peptide by scrambled peptide without HER2-binding

activity (TPM5 control group) resulted in loss of both nanofibril transformation property and anti-tumour activity, confirming the importance of ligand–receptor interaction in this *in situ* transformable nanotechnology (Supplementary Fig. 37). We believe that the cell surface receptor-mediated transformable peptide nanoplatform has great clinical potential.

Online content

Any methods, additional references, Nature Research reporting summaries, source data, extended data, supplementary information, acknowledgements, peer review information; details of author contributions and competing interests; and statements of data and code availability are available at <https://doi.org/10.1038/s41565-019-0626-4>.

Received: 11 February 2019; Accepted: 27 November 2019;

Published online: 27 January 2020

References

- Slamon, D. J. et al. Human breast cancer: correlation of relapse and survival with amplification of the HER-2/neu oncogene. *Science* **235**, 177–182 (1987).
- Arteaga, C. L. et al. Treatment of HER2-positive breast cancer: current status and future perspectives. *Nat. Rev. Clin. Oncol.* **9**, 16–32 (2011).
- Gravalos, C. & Jimeno, A. HER2 in gastric cancer: a new prognostic factor and a novel therapeutic target. *Ann. Oncol.* **19**, 1523–1529 (2008).
- Ferte, C., Andre, F. & Soria, J. C. Molecular circuits of solid tumours: prognostic and predictive tools for bedside use. *Nat. Rev. Clin. Oncol.* **7**, 367–380 (2010).
- Roukos, D. H. & Briasoulis, E. Individualized preventive and therapeutic management of hereditary breast ovarian cancer syndrome. *Nat. Clin. Pract. Oncol.* **4**, 578–590 (2007).
- Kantarjian, H. et al. Hematologic and cytogenetic responses to imatinib mesylate in chronic myelogenous leukemia. *N. Engl. J. Med.* **346**, 645–652 (2002).
- Jänne, P. A. & Johnson, B. E. Effect of epidermal growth factor receptor tyrosine kinase domain mutations on the outcome of patients with non-small cell lung cancer treated with epidermal growth factor receptor tyrosine kinase inhibitors. *Clin. Cancer Res.* **12**, 4416s–4420s (2006).
- Ferguson, K. M. Structure-based view of epidermal growth factor receptor regulation. *Annu. Rev. Biophys.* **37**, 353–373 (2008).
- Ruiz-Saenz, A. & Moasser, M. M. Targeting HER2 by combination therapies. *J. Clin. Oncol.* **36**, 808–811 (2018).
- Zhang, X., Gureasko, J., Shen, K., Cole, P. A. & Kuriyan, J. An allosteric mechanism for activation of the kinase domain of epidermal growth factor receptor. *Cell* **125**, 1137–1149 (2006).
- Olayioye, M. A., Neve, R. M., Lane, H. A. & Hynes, N. E. The ErbB signaling network: receptor heterodimerization in development and cancer. *EMBO J.* **19**, 3159–3167 (2000).
- Gschwind, A., Fischer, O. M. & Ullrich, A. The discovery of receptor tyrosine kinases: targets for cancer therapy. *Nat. Rev. Cancer* **4**, 361–370 (2004).
- Shin, Y. & Brangwynne, C. P. Liquid phase condensation in cell physiology and disease. *Science* **357**, eaaf4382 (2017).
- Li, Y., Wang, Y., Huang, G. & Gao, J. Cooperativity principles in self-assembled nanomedicine. *Chem. Rev.* **118**, 5359–5391 (2018).
- Mattia, E. & Otto, S. Supramolecular systems chemistry. *Nat. Nanotechnol.* **10**, 111–119 (2015).
- Webber, M. J., Appel, E. A., Meijer, E. & Langer, R. Supramolecular biomaterials. *Nat. Mater.* **15**, 13–26 (2016).
- Haburcak, R., Shi, J., Du, X., Yuan, D. & Xu, B. Ligand–receptor interaction modulates the energy landscape of enzyme-instructed self-assembly of small molecules. *J. Am. Chem. Soc.* **138**, 15397–15404 (2016).
- Feng, Z., Wang, H., Chen, X. & Xu, B. Self-assembling ability determines the activity of enzyme-instructed self-assembly for inhibiting cancer cells. *J. Am. Chem. Soc.* **139**, 15377–15384 (2017).
- Li, J. et al. Selection of secondary structures of heterotypic supramolecular peptide assemblies by an enzymatic reaction. *Angew. Chem. Int. Ed.* **57**, 11716–11721 (2018).
- He, P. P., Li, X. D., Wang, L. & Wang, H. Bispyrene-based self-assembled nanomaterials: *in vivo* self-assembly, transformation, and biomedical effects. *Acc. Chem. Res.* **52**, 367–378 (2019).
- Qi, G. B., Gao, Y. J., Wang, L. & Wang, H. Self-assembled peptide-based nanomaterials for biomedical imaging and therapy. *Adv. Mater.* **30**, 1703444 (2018).
- Yang, P. P. et al. Host materials transformable in tumour microenvironment for homing theranostics. *Adv. Mater.* **29**, 1605869 (2017).

23. Tan, J. et al. Role of CD40 ligand in amyloidosis in transgenic Alzheimer's mice. *Nat. Neurosci.* **5**, 1288–1293 (2002).
24. Hock, C. et al. Generation of antibodies specific for β -amyloid by vaccination of patients with Alzheimer disease. *Nat. Med.* **8**, 1270–1275 (2002).
25. Park, B. W. et al. Rationally designed anti-HER2/neu peptide mimetic disables P185HER2/neu tyrosine kinases *in vitro* and *in vivo*. *Nat. Biotechnol.* **18**, 194–198 (2000).
26. Berezov, A., Zhang, H. T., Greene, M. I. & Murali, R. Disabling erbB receptors with rationally designed exocyclic mimetics of antibodies: structure–function analysis. *J. Med. Chem.* **44**, 2565–2574 (2001).
27. Kitagawa, K. & Abdulle, R. Deoxycholate-based method to screen phage display clones for uninterrupted open reading frames. *Mol. Cell* **4**, 21–33 (1995).
28. Kaiser, T. E., Wang, H., Stepanenko, V. & Würthner, F. Supramolecular construction of fluorescent J-aggregates based on hydrogen-bonded perylene dyes. *Angew. Chem. Int. Ed.* **119**, 5637–5640 (2007).
29. Hu, X.-X. et al. Transformable nanomaterials as an artificial extracellular matrix for inhibiting tumour invasion and metastasis. *ACS Nano* **11**, 4086–4096 (2017).
30. Korevaar, P. A. et al. Pathway complexity in supramolecular polymerization. *Nature* **481**, 492–496 (2012).
31. Zagar, T. M., Cardinale, D. M. & Marks, L. B. Breast cancer therapy-associated cardiovascular disease. *Nat. Rev. Clin. Oncol.* **13**, 172–184 (2016).
32. Duru, N. et al. HER2-associated radioresistance of breast cancer stem cells isolated from HER2-negative breast cancer cells. *Clin. Cancer Res.* **18**, 6634–6647 (2012).
33. Adams, S. R. et al. Anti-tubulin drugs conjugated to anti-ErbB antibodies selectively radiosensitize. *Nat. Commun.* **7**, 13019 (2016).
34. Chang, L. et al. Proteomics discovery of radioresistant cancer biomarkers for radiotherapy. *Cancer Lett.* **369**, 289–297 (2015).
35. Kuang, Y. et al. Pericellular hydrogel/nanonets inhibit cancer cells. *Angew. Chem. Int. Ed.* **53**, 8104–8107 (2014).
36. Pires, R. A. et al. Controlling cancer cell fate using localized biocatalytic self-assembly of an aromatic carbohydrate amphiphile. *J. Am. Chem. Soc.* **137**, 576–579 (2015).
37. Jeena, M. T. et al. Mitochondria localization induced self-assembly of peptide amphiphiles for cellular dysfunction. *Nat. Commun.* **8**, 26 (2017).
38. Zhang, D. et al. *In situ* formation of nanofibers from purpurin18-peptide conjugates and the assembly induced retention effect in tumour sites. *Adv. Mater.* **27**, 6125–6130 (2015).
39. Tanaka, A. et al. Cancer cell death induced by the intracellular self-assembly of an enzyme-responsive supramolecular gelator. *J. Am. Chem. Soc.* **137**, 770–775 (2015).
40. Wang, H.-J. et al. JMJD5 regulates PKM2 nuclear translocation and reprograms HIF-1 α -mediated glucose metabolism. *Proc. Natl Acad. Sci. USA* **111**, 279–284 (2014).
41. Mariani, G., Fasolo, A., De Benedictis, E. & Gianni, L. Trastuzumab as adjuvant systemic therapy for HER2-positive breast cancer. *Nat. Clin. Pract. Oncol.* **6**, 93–104 (2009).
42. Popat, S. & Smith, I. E. Therapy insight: anthracyclines and trastuzumab—the optimal management of cardiotoxic side effects. *Nat. Rev. Clin. Oncol.* **5**, 324–325 (2008).
43. Xiao, W. et al. Discovery and characterization of a high-affinity and high-specificity peptide ligand LXY30 for *in vivo* targeting of $\alpha 3$ integrin-expressing human tumours. *Ejmmi. Res.* **6**, 18 (2016).

Publisher's note Springer Nature remains neutral with regard to jurisdictional claims in published maps and institutional affiliations.

© The Author(s), under exclusive licence to Springer Nature Limited 2020

Methods

Preparation of TPM1–4. The hydrophobic bis-pyrene unit (*BP*-COOH) was synthesized according to a previous report⁴⁴. TPM1–4 were synthesized by standard solid-phase peptide synthesis techniques. *BP*-COOH as a hydrophobic unit was linked to the TPM1–4 chain. For TPM3 and 4, PEG₁₀₀₀ as a hydrophilic unit was linked to the peptide to replace the HER2 ligand of TPM1 and 2. The molecular structures of *BP* dye and peptides were confirmed by matrix-assisted laser desorption ionization time-of-flight mass spectrometry (ESI and MALDI-TOF mass spectra, Bruker Daltonics).

Self-assembly preparation and characterization of NPs. Transformable peptide monomers 1–4 were dissolved in DMSO to form a solution. Peptide solution (5 μ l) was further diluted with DMSO (995, 795, 595, 395, 195, 95, 15 and 0 μ l) and mixed with deionized water (0, 200, 400, 600, 800, 900, 980 and 995 μ l). The ultraviolet-visible (UV-vis) absorption and fluorescence spectra (UV-1800, Shimadzu and RF6000, Shimadzu) of solutions with varying water content were measured to validate the formation of NPs. Fresh NPs (99% water content, 20 μ M) were used for measurement as an initial state. The morphology transformation of NPs to NFs was performed by the addition of HER2 extracellular receptor protein (expressed in HEK 293 cells, Sigma-Aldrich) and cultured for several hours at 37 °C. At different time points (0.5, 6 and 24 h) the solution was used for size/zeta potential (DLS, Nano ZS), circular dichroism (JASCO) and TEM measurement (CM-120 TEM, Phillips). TEM samples were dyed with uranyl acetate. Pyrene molecules were employed as an indicator to determine the CAC of nanoparticles, by comparing the fluorescence of their third and first emissive peaks. First, NPs were diluted to different concentrations (0.01, 0.05, 0.1, 0.5, 1, 5, 10, 20, 30 and 50 μ M), then 999 μ l of NPs of each dilution was incubated with 1 μ l of pyrene acetone solution (0.1 mM) at 37 °C for 2 h. The fluorescence spectra of pyrene (excitation, 335 nm) in different NPs dilutions were recorded. The fluorescence intensity ratio (I3/I1) of the third and first emissive peaks was measured for CAC calculation.

Stability of NPs1–4 in the presence of human plasma and protease. The stability of NPs1–4 was studied in 10% (v/v) plasma from healthy human volunteers, and in protease solution. The mixture was incubated at physiological body temperature (37 °C) followed by size measurements at predetermined time intervals up to 168 h. Finally, the high-performance liquid chromatography spectra of NPs (300 μ M) with protease (2 mg ml⁻¹) after 7 d were recorded.

Cell lines. MCF-7, SKBR-3 and BT474 cells were purchased from the American Type Culture Collection. The induction method of MCF-7/C6 cells was obtained from the laboratory of J. J. Li (Departments of Radiation Oncology, University of California Davis). The MCF-7/C6 radioresistant cell line was created following 25 fractionated ionizing radiation sessions with a total dose of 50 Gy γ -rays (2 Gy per fraction, five times per week). A short tandem-repeat DNA profiling method was used to authenticate the cell lines, and the results were compared to the reference database. No Mycoplasma contamination was detected in the above cell lines.

Confocal laser scanning microscopy and SEM validation of NPs structural transformation on cell surfaces. Cells were cultured in glass-bottom dishes for 12 h. NPs1–4 (50 μ M) were incubated with cells in DMEM at 37 °C for 0.5, 6, 24 and 48 h, respectively. For confocal laser scanning microscopy imaging (LSM 800, ZEISS), specimens were solidified with glutaraldehyde (4%) for 10 min, washed with PBS three times and examined with either a \times 40 or \times 63 immersion objective lens and a 405-nm laser. To further validate the binding of NPs1 to HER2, we used rabbit anti-HER2 (29D8) monoclonal antibody (Sigma-Aldrich) to detect the extracellular domain of HER2 on the surface of MCF-7/C6 cells. For SEM (Phillips XL30 TMP, FEI), cells were solidified with glutaraldehyde (4%) overnight and then coated with gold for 2 min.

In vitro cytotoxic assay. MCF-7/C6, MCF-7, SKBR-3 and BT474 cells were used to evaluate the cytotoxicity of NPs1–4. Cells were seeded in 96-well plates ($n=3$), cultured with DMEM and supplemented with 10% FBS and 1% penicillin at 37 °C in a humidified environment containing 5% CO₂. A 1/4 DMSO solution was diluted by DMEM (1.5, 7.5, 15, 75, 150 and 300 μ M) and then added to each well for incubation with cells. After 48 h of incubation, MTS reagent was added to each well. Relative cell viability was measured using a micro-plate reader (SpectraMax M3). Percentage cell viability represented drug effect, with 100% denoting that all cells survived. Cell viability was calculated by measuring the optical density (OD₄₉₀) of MTS formazan using the following equation: cell viability (%) = (OD₄₉₀ treatment/OD₄₉₀ blank control) \times 100.

Immunoblot analysis. MCF-7/C6 cells were treated under different conditions, collected by centrifugation at 14,000 r.p.m. for 10 min and lysed with 1% (v/v) Triton X-100 containing lysis buffer (50 mM Tris-HCl, pH 8.0, 150 mM NaCl) with protease inhibitor. Total cellular proteins were estimated using a BCA kit (Applygen). Each sample (50 μ g of protein) was subjected to SDS-PAGE and transferred to nitrocellulose membranes. After blocking for 2 h at room temperature with 5% (wt/v) non-fat dry milk in Blotto solution (20 mM Tris-HCl, pH 7.5, 150 mM NaCl and 0.1% Tween 20), the membranes were incubated

with primary antibody overnight at 4 °C. The membranes were then washed (3 \times 5 min) with Tris buffered saline and Tween and incubated with a second round of antibodies for 2 h at room temperature. Signals were visualized by chemiluminescence on a Typhoon Trio Variable Mode Imager. Band density was calculated using NIH Image J software.

HER2 dimer analysis used with immunoblot has previously been described⁴⁰. Briefly, HER2 high-expression MCF-7/C6 cells were treated with NPs1 or other drugs, as indicated by previous protocols, and lysed in 1.0% Triton X-100 buffer (pH 7.4) containing 137 mM NaCl, 2.7 mM KCl, 10 mM Na₂HPO₄, 1.8 mM KH₂PO₄ and a protease inhibitor cocktail (Sigma-Aldrich) for 30 min at 4 °C. For performance of cross-linking reactions, the lysis supernatant was collected after centrifugation at 12,000 r.p.m. for 15 min; 0.2% glutaraldehyde was added to the lysis supernatant, giving a final concentration of 0.01%, for 10 min at 37 °C. Reactions were terminated by the addition of 1 M Tris buffer to give a final concentration of 50 mM Tris-Cl (pH 8.0). Samples were then separated by 6% SDS-PAGE and analysed by immunoblotting with anti-HER2 or other antibodies as indicated.

Animal maintenance. All animal experiments were performed in accordance with protocol No.19724, which was approved by the Animal Use and Care Administrative Advisory Committee at the University of California, Davis. Experiments were carried out in accordance with the relevant guidelines and ethical regulations. The jugular vein of male Sprague-Dawley rats was cannulated, and a catheter implanted for IV injection and blood collection (Harland). NPs (8 mg kg⁻¹) were administered IV to rats ($n=3$). Whole-blood samples (~100 μ l) were collected from the jugular vein catheter before dosing and at predetermined time points post-injection. Fluorescence of samples for the standard curve and each experimental group was measured following the dilution of blood serum sample with PBS (serum/PBS, 20/80, vol%). Female Balb/c nude mice (aged 6–8 weeks, weight, 22 \pm 2 g) were purchased from Envigo. MCF-7/C6 cells (5 \times 10⁶ cells per mouse) were inoculated subcutaneously into the flank of each female mouse. After around 10 d, NPs1–4 (8 mg kg⁻¹) were injected via the tail vein and ex vivo images of tumour, heart, liver, spleen, lung, kidney, intestine, muscle and skin were collected at 10, 24, 48, 72 and 168 h post-injection. Images were collected by an in vivo fluorescence imaging system (In-Vivo Imaging System FXPRO, Carestream). Both tumour and key organs (heart, liver, spleen, lung, kidney and brain) were collected and solidified with glutaraldehyde (4%) at 72 h post-injection of NPs, for TEM imaging.

In vivo therapeutic effect. Balb/c nude mice with MCF-7/C6 tumour cells (5 \times 10⁶ cells per mouse) inoculated subcutaneously into the flank were used in our experiments. The mice were randomly divided into five groups at 10 d post-tumour inoculation. Each was treated with PBS, NPs1, NPs2, NPs3 or NPs4 every 48 h by IV administration. During the treatment period (40 d) tumour volume and body weight were measured twice per week. For haematoxylin and eosin (H&E) and Ki-67 staining procedures, MCF-7/C6 tumour-bearing mice were sacrificed after three treatments and tumour tissues were collected. In parallel, the therapeutic effect of NPs1 was verified in mice bearing SKBR-3 or BT474 tumours, similarly to the experimental method above. For the BT474 model, mice were pre-implanted with a 17- β -oestradiol pellet.

Statistical analysis. Data are presented as mean \pm s.d. Intergroup comparison was analysed by Student's *t*-test (two-tailed). One-way analysis of variance (ANOVA) was used for multiple-group analysis. The level of significance was defined as **P* < 0.05, ***P* < 0.01 and ****P* < 0.001. All statistical tests were two-sided.

Reporting Summary. Further information on research design is available in the Nature Research Reporting Summary linked to this article.

Data availability

All data generated or analysed during this study are available in this published article and its Supplementary Information files or from the corresponding author on request.

References

- Qiao, S.-L. et al. Thermo-controlled *in situ* phase transition of polymer-peptides on cell surfaces for high-performance proliferative inhibition. *ACS Appl. Mater. Interfaces* **8**, 17016–17022 (2016).

Acknowledgements

This work was supported in part by NIH/NCI (grant nos. R01CA115483, U01CA198880, R01CA199668 and R01CA232845), NIH/NIBIB (grant no. R01EB012569), NIH/NICHD (grant no. R01HD086195) and the National Natural Science Foundation of China (grant no. 51573101).

Author contributions

K.S.L., L.W. and L.Z. conceived the idea and developed the project. L.Z. conducted all experiments and analysed data. Z.C. and T.R. assisted with chemical synthesis and data analysis. D.J., T.R., C.M.B., N.J. and D.Z. assisted with cell culture studies. D.J., W.X., Y.W., N.J. and Z.C. assisted with animal studies. J.J.L. provided MCF-7/C6 and 4T1/HER2 cell

lines and the background knowledge on HER2⁺ breast cancer. Y.L. assisted with design and supervision of the research. K.S.L., L.W. and L.Z. co-wrote the paper and all authors commented on the manuscript. K.S.L. supervised the whole project.

Competing interests

The authors declare the following competing interests. K.S.L., L.Z., D.J. and L.W. are co-inventors of a pending patent on fibrillar-transformable nanoparticles. K.S.L. is the founding scientist of LamnoTherapeutics Inc., which plans to develop the nanotherapeutics described in the manuscript. The remaining authors declare no competing interests.

Additional information

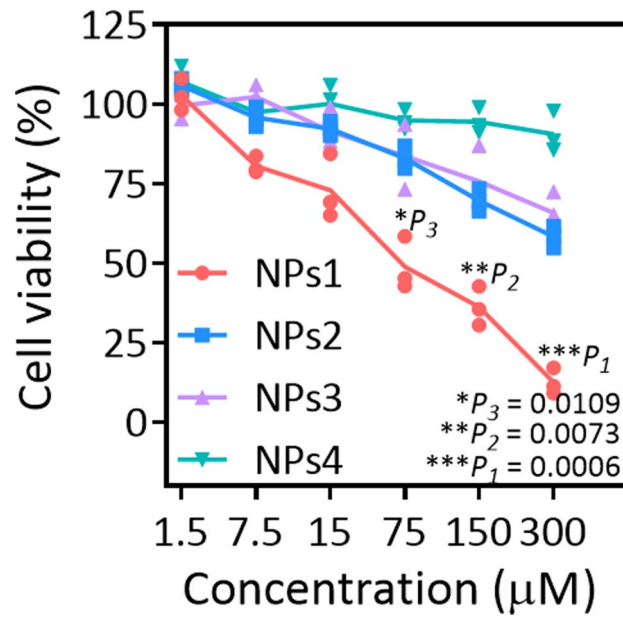
Extended data is available for this paper at <https://doi.org/10.1038/s41565-019-0626-4>.

Supplementary information is available for this paper at <https://doi.org/10.1038/s41565-019-0626-4>.

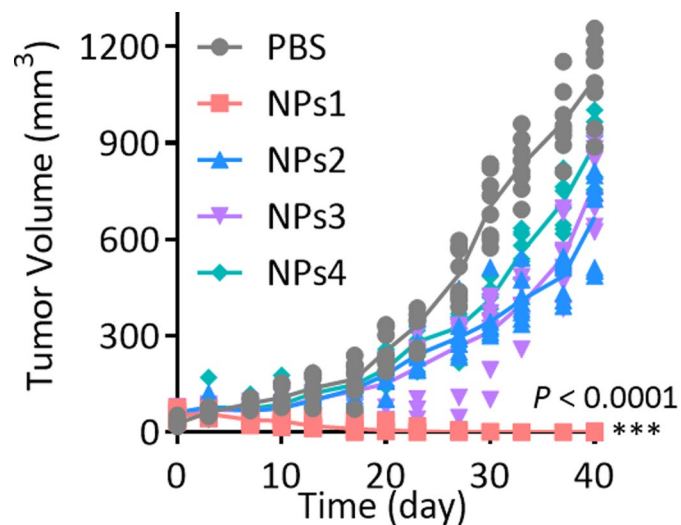
Correspondence and requests for materials should be addressed to L.W. or K.S.L.

Peer review information *Nature Nanotechnology* thanks Jinming Gao, Maurizio Scaltriti and the other, anonymous, reviewer(s) for their contribution to the peer review of this work.

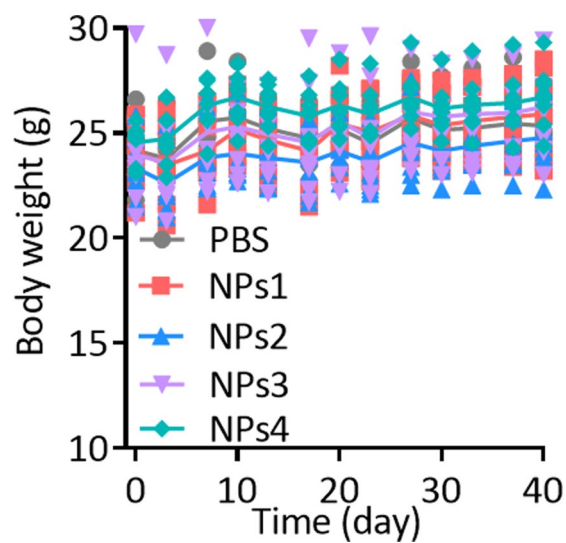
Reprints and permissions information is available at www.nature.com/reprints.



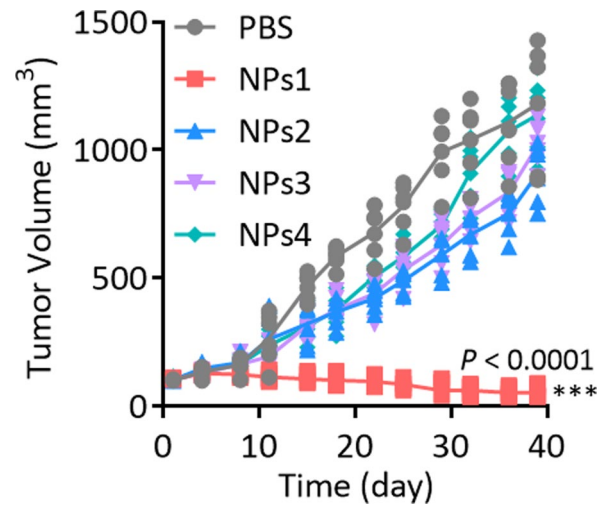
Extended Data Fig. 1 | Figure 3b with the original points. The viability of MCF-7/C6 cells after incubation with NPs1-4 at the different concentration for 48 h. Data are presented as the mean \pm s.d., $n=3$ independent experiments. The statistical significance was calculated via a one-way analysis of variance (ANOVA) with a Tukey post-hoc test. * $P < 0.05$, ** $P < 0.01$, *** $P < 0.001$.



Extended Data Fig. 2 | Figure 5b with the original points. Observation of the tumour inhibition effect of mice in subcutaneous tumour model during the 40 days of treatment ($n = 8$ per group; the dose of NPs1-4 were 8 mg/kg per injection). Data are presented as the mean \pm s.d. The statistical significance was calculated *via* a one-way ANOVA with a Tukey post-hoc test. *** $P < 0.001$.



Extended Data Fig. 3 | Figure 5c with the original points. Observation of weight change of mice in subcutaneous tumour model during the 40 days of treatment ($n = 8$ per group; the dose of NPs1-4 were 8 mg/kg per injection). Data are presented as the mean \pm s.d.



Extended Data Fig. 4 | Figure 5j with the original points. Observation of the tumour inhibition effect in subcutaneous BT474 HER2 positive breast cancer models during the 40 days of treatment ($n = 6$ per group; the dose of NPs1-4 were 8 mg/kg per injection). Data are presented as the mean \pm s.d. The statistical significance was calculated via a one-way ANOVA with a Tukey post-hoc test. *** $P < 0.001$.

Reporting Summary

Nature Research wishes to improve the reproducibility of the work that we publish. This form provides structure for consistency and transparency in reporting. For further information on Nature Research policies, see [Authors & Referees](#) and the [Editorial Policy Checklist](#).

Statistics

For all statistical analyses, confirm that the following items are present in the figure legend, table legend, main text, or Methods section.

n/a Confirmed

- The exact sample size (n) for each experimental group/condition, given as a discrete number and unit of measurement
- A statement on whether measurements were taken from distinct samples or whether the same sample was measured repeatedly
- The statistical test(s) used AND whether they are one- or two-sided
Only common tests should be described solely by name; describe more complex techniques in the Methods section.
- A description of all covariates tested
- A description of any assumptions or corrections, such as tests of normality and adjustment for multiple comparisons
- A full description of the statistical parameters including central tendency (e.g. means) or other basic estimates (e.g. regression coefficient) AND variation (e.g. standard deviation) or associated estimates of uncertainty (e.g. confidence intervals)
- For null hypothesis testing, the test statistic (e.g. F , t , r) with confidence intervals, effect sizes, degrees of freedom and P value noted
Give P values as exact values whenever suitable.
- For Bayesian analysis, information on the choice of priors and Markov chain Monte Carlo settings
- For hierarchical and complex designs, identification of the appropriate level for tests and full reporting of outcomes
- Estimates of effect sizes (e.g. Cohen's d , Pearson's r), indicating how they were calculated

Our web collection on [statistics for biologists](#) contains articles on many of the points above.

Software and code

Policy information about [availability of computer code](#)

Data collection

Gatan Microscopy Suite 3 on Transmission electron microscopy (Philips CM-120 TEM, America); Zetasizer on Dynamic light scattering instrument (DLS, Nano ZS, Malvern); UVProbe2.52 on UV-vis photospectrometer (UV-1800, Shimadzu); LabSolutions RF on Fluorescence photospectrometer (RF6000, Shimadzu); Circular dichroism spectropolarimeter (JASCO Inc, Easton, MD, USA); Carestream MI SE on Kodak multimodal imaging system (IS2000MM); Confocal laser scanning microscopy (LSM 800, ZEISS); Scanning electron microscope (Philips XL30 TMP, FEI Company, The Netherlands); Microplate reader (SpectraMax M3, USA); High performance liquid chromatography (HPLC, 1200 series, Agilent Technologies); Mass spectrometry (MS, 6420 triple Quad, Agilent Technologies), with 1200 series HPLC system, Agilent Technologies); Matrix Assisted Laser Desorption/Ionization-Time of Flight Mass Spectrometry (ESI and MALDI-TOF MS, UltraFLEXtreme, Bruker).

Data analysis

Bar graph, curves and the relevant statistics were analyzed by GraphPad Prism 8.0 and origin 9.0; Confocal data were analyzed by ZEN 2.3; Western blot images were analyzed by ImageJ 1.52g.

For manuscripts utilizing custom algorithms or software that are central to the research but not yet described in published literature, software must be made available to editors/reviewers. We strongly encourage code deposition in a community repository (e.g. GitHub). See the Nature Research [guidelines for submitting code & software](#) for further information.

Data

Policy information about [availability of data](#)

All manuscripts must include a [data availability statement](#). This statement should provide the following information, where applicable:

- Accession codes, unique identifiers, or web links for publicly available datasets
- A list of figures that have associated raw data
- A description of any restrictions on data availability

All the primary data that support the findings of this study are available from the corresponding author on request.

Field-specific reporting

Please select the one below that is the best fit for your research. If you are not sure, read the appropriate sections before making your selection.

Life sciences Behavioural & social sciences Ecological, evolutionary & environmental sciences

For a reference copy of the document with all sections, see [nature.com/documents/nr-reporting-summary-flat.pdf](https://www.nature.com/documents/nr-reporting-summary-flat.pdf)

Life sciences study design

All studies must disclose on these points even when the disclosure is negative.

Sample size	Sample sizes were based on our previous experience and other publications. The sample size was at least that of a triplicate, providing enough statistical power to detect the usually strong effects observed in our experiments. All sample sizes are clearly described in the manuscript or the figure legends.
Data exclusions	No data were excluded from the analyses.
Replication	All experiments were replicated at least twice (i.e. $n \geq 3$ biological replicates) with similar results. All attempts at replication were successful.
Randomization	All samples were allocated to groups randomly.
Blinding	For the in vivo end-point evaluations, the investigators were blinded to group allocation during data collection and analysis.

Behavioural & social sciences study design

All studies must disclose on these points even when the disclosure is negative.

Study description	Briefly describe the study type including whether data are quantitative, qualitative, or mixed-methods (e.g. qualitative cross-sectional, quantitative experimental, mixed-methods case study).
Research sample	State the research sample (e.g. Harvard university undergraduates, villagers in rural India) and provide relevant demographic information (e.g. age, sex) and indicate whether the sample is representative. Provide a rationale for the study sample chosen. For studies involving existing datasets, please describe the dataset and source.
Sampling strategy	Describe the sampling procedure (e.g. random, snowball, stratified, convenience). Describe the statistical methods that were used to predetermine sample size OR if no sample-size calculation was performed, describe how sample sizes were chosen and provide a rationale for why these sample sizes are sufficient. For qualitative data, please indicate whether data saturation was considered, and what criteria were used to decide that no further sampling was needed.
Data collection	Provide details about the data collection procedure, including the instruments or devices used to record the data (e.g. pen and paper, computer, eye tracker, video or audio equipment) whether anyone was present besides the participant(s) and the researcher, and whether the researcher was blind to experimental condition and/or the study hypothesis during data collection.
Timing	Indicate the start and stop dates of data collection. If there is a gap between collection periods, state the dates for each sample cohort.
Data exclusions	If no data were excluded from the analyses, state so OR if data were excluded, provide the exact number of exclusions and the rationale behind them, indicating whether exclusion criteria were pre-established.
Non-participation	State how many participants dropped out/declined participation and the reason(s) given OR provide response rate OR state that no participants dropped out/declined participation.
Randomization	If participants were not allocated into experimental groups, state so OR describe how participants were allocated to groups, and if allocation was not random, describe how covariates were controlled.

Ecological, evolutionary & environmental sciences study design

All studies must disclose on these points even when the disclosure is negative.

Study description	Briefly describe the study. For quantitative data include treatment factors and interactions, design structure (e.g. factorial, nested, hierarchical), nature and number of experimental units and replicates.
Research sample	Describe the research sample (e.g. a group of tagged <i>Passer domesticus</i> , all <i>Stenocereus thurberi</i> within Organ Pipe Cactus National Monument), and provide a rationale for the sample choice. When relevant, describe the organism taxa, source, sex, age range and any manipulations. State what population the sample is meant to represent when applicable. For studies involving existing datasets,

describe the data and its source.

Sampling strategy *Note the sampling procedure. Describe the statistical methods that were used to predetermine sample size OR if no sample-size calculation was performed, describe how sample sizes were chosen and provide a rationale for why these sample sizes are sufficient.*

Data collection *Describe the data collection procedure, including who recorded the data and how.*

Timing and spatial scale *Indicate the start and stop dates of data collection, noting the frequency and periodicity of sampling and providing a rationale for these choices. If there is a gap between collection periods, state the dates for each sample cohort. Specify the spatial scale from which the data are taken*

Data exclusions *If no data were excluded from the analyses, state so OR if data were excluded, describe the exclusions and the rationale behind them, indicating whether exclusion criteria were pre-established.*

Reproducibility *Describe the measures taken to verify the reproducibility of experimental findings. For each experiment, note whether any attempts to repeat the experiment failed OR state that all attempts to repeat the experiment were successful.*

Randomization *Describe how samples/organisms/participants were allocated into groups. If allocation was not random, describe how covariates were controlled. If this is not relevant to your study, explain why.*

Blinding *Describe the extent of blinding used during data acquisition and analysis. If blinding was not possible, describe why OR explain why blinding was not relevant to your study.*

Did the study involve field work? Yes No

Field work, collection and transport

Field conditions *Describe the study conditions for field work, providing relevant parameters (e.g. temperature, rainfall).*

Location *State the location of the sampling or experiment, providing relevant parameters (e.g. latitude and longitude, elevation, water depth).*

Access and import/export *Describe the efforts you have made to access habitats and to collect and import/export your samples in a responsible manner and in compliance with local, national and international laws, noting any permits that were obtained (give the name of the issuing authority, the date of issue, and any identifying information).*

Disturbance *Describe any disturbance caused by the study and how it was minimized.*

Reporting for specific materials, systems and methods

We require information from authors about some types of materials, experimental systems and methods used in many studies. Here, indicate whether each material, system or method listed is relevant to your study. If you are not sure if a list item applies to your research, read the appropriate section before selecting a response.

Materials & experimental systems

n/a	Involvement in the study
<input type="checkbox"/>	<input checked="" type="checkbox"/> Antibodies
<input type="checkbox"/>	<input checked="" type="checkbox"/> Eukaryotic cell lines
<input checked="" type="checkbox"/>	<input type="checkbox"/> Palaeontology
<input type="checkbox"/>	<input checked="" type="checkbox"/> Animals and other organisms
<input checked="" type="checkbox"/>	<input type="checkbox"/> Human research participants
<input checked="" type="checkbox"/>	<input type="checkbox"/> Clinical data

Methods

n/a	Involvement in the study
<input checked="" type="checkbox"/>	<input type="checkbox"/> ChIP-seq
<input checked="" type="checkbox"/>	<input type="checkbox"/> Flow cytometry
<input checked="" type="checkbox"/>	<input type="checkbox"/> MRI-based neuroimaging

Antibodies

Antibodies used

The following primary antibodies were used for western blotting. All the antibodies were diluted and used following the supplier protocol.

Phospho-p44/42 MAPK (Erk1/2), Cell Signaling Technology, catalog: #4370;
 p44/42 MAPK (Erk1/2), Cell Signaling Technology, catalog: #4695;
 MEK1/2, Cell Signaling Technology, catalog: #8727;
 Phospho-MEK, Cell Signaling Technology, catalog: #9127;
 c-Raf, Cell Signaling Technology, catalog: #9422;
 Phospho-c-Raf (Ser338), Cell Signaling Technology, catalog: #9427;
 HER2, Santa cruz biotechnology, catalog: #sc-284;
 Bcl-2, Santa cruz biotechnology, catalog: #sc-130308;
 Bax, Santa cruz biotechnology, catalog: #sc-493;
 Tubulin, Sigma Aldrich; catalog: #T6074;
 Actin, Cell Signaling Technology, catalog: #3700.

The following primary antibody was used for immunofluorescence.
HER2/ErbB2 (29D8) Rabbit antibody, Cell Signaling Technology, catalog: #2165;
Secondary Antibody, Alexa Fluor 555, ThermoFisher Scientific, catalog: #A-21428

Validation

All antibodies were verified by the supplier and each lot has been quality tested.

Eukaryotic cell lines

Policy information about [cell lines](#)

Cell line source(s)

MCF-7/C6 cell line was kindly provided by Dr. Jian Jian Li's Lab. MCF-7, SKBR-3 and BT474 cell lines were purchased from American Type Culture Collection.

Authentication

Cell line authentication was performed by short tandem repeat DNA profiling.

Mycoplasma contamination

All cell lines were tested for mycoplasma contamination. No mycoplasma contamination was found.

Commonly misidentified lines
(See [ICLAC](#) register)

There were no commonly misidentified lines used in this study.

Palaeontology

Specimen provenance

Provide provenance information for specimens and describe permits that were obtained for the work (including the name of the issuing authority, the date of issue, and any identifying information).

Specimen deposition

Indicate where the specimens have been deposited to permit free access by other researchers.

Dating methods

If new dates are provided, describe how they were obtained (e.g. collection, storage, sample pretreatment and measurement), where they were obtained (i.e. lab name), the calibration program and the protocol for quality assurance OR state that no new dates are provided.

Tick this box to confirm that the raw and calibrated dates are available in the paper or in Supplementary Information.

Animals and other organisms

Policy information about [studies involving animals](#); [ARRIVE guidelines](#) recommended for reporting animal research

Laboratory animals

Female BALB/c nude mice (6-8 week).

Wild animals

The study did not involve wild animals.

Field-collected samples

This study did not involve samples collected from the fields

Ethics oversight

All animal experiments were in accordance with protocols No.19724, which was approved by the Animal Use and Care Administrative Advisory Committee at the University of California, Davis.

Note that full information on the approval of the study protocol must also be provided in the manuscript.

Human research participants

Policy information about [studies involving human research participants](#)

Population characteristics

Describe the covariate-relevant population characteristics of the human research participants (e.g. age, gender, genotypic information, past and current diagnosis and treatment categories). If you filled out the behavioural & social sciences study design questions and have nothing to add here, write "See above."

Recruitment

Describe how participants were recruited. Outline any potential self-selection bias or other biases that may be present and how these are likely to impact results.

Ethics oversight

Identify the organization(s) that approved the study protocol.

Note that full information on the approval of the study protocol must also be provided in the manuscript.

Clinical data

Policy information about [clinical studies](#)

All manuscripts should comply with the ICMJE [guidelines for publication of clinical research](#) and a completed [CONSORT checklist](#) must be included with all submissions.

Clinical trial registration

Provide the trial registration number from ClinicalTrials.gov or an equivalent agency.

Study protocol	<i>Note where the full trial protocol can be accessed OR if not available, explain why.</i>
Data collection	<i>Describe the settings and locales of data collection, noting the time periods of recruitment and data collection.</i>
Outcomes	<i>Describe how you pre-defined primary and secondary outcome measures and how you assessed these measures.</i>

ChIP-seq

Data deposition

- Confirm that both raw and final processed data have been deposited in a public database such as [GEO](#).
- Confirm that you have deposited or provided access to graph files (e.g. BED files) for the called peaks.

Data access links <i>May remain private before publication.</i>	<i>For "Initial submission" or "Revised version" documents, provide reviewer access links. For your "Final submission" document, provide a link to the deposited data.</i>
Files in database submission	<i>Provide a list of all files available in the database submission.</i>
Genome browser session (e.g. UCSC)	<i>Provide a link to an anonymized genome browser session for "Initial submission" and "Revised version" documents only, to enable peer review. Write "no longer applicable" for "Final submission" documents.</i>

Methodology

Replicates	<i>Describe the experimental replicates, specifying number, type and replicate agreement.</i>
Sequencing depth	<i>Describe the sequencing depth for each experiment, providing the total number of reads, uniquely mapped reads, length of reads and whether they were paired- or single-end.</i>
Antibodies	<i>Describe the antibodies used for the ChIP-seq experiments; as applicable, provide supplier name, catalog number, clone name, and lot number.</i>
Peak calling parameters	<i>Specify the command line program and parameters used for read mapping and peak calling, including the ChIP, control and index files used.</i>
Data quality	<i>Describe the methods used to ensure data quality in full detail, including how many peaks are at FDR 5% and above 5-fold enrichment.</i>
Software	<i>Describe the software used to collect and analyze the ChIP-seq data. For custom code that has been deposited into a community repository, provide accession details.</i>

Flow Cytometry

Plots

- Confirm that:
- The axis labels state the marker and fluorochrome used (e.g. CD4-FITC).
- The axis scales are clearly visible. Include numbers along axes only for bottom left plot of group (a 'group' is an analysis of identical markers).
- All plots are contour plots with outliers or pseudocolor plots.
- A numerical value for number of cells or percentage (with statistics) is provided.

Methodology

Sample preparation	<i>Describe the sample preparation, detailing the biological source of the cells and any tissue processing steps used.</i>
Instrument	<i>Identify the instrument used for data collection, specifying make and model number.</i>
Software	<i>Describe the software used to collect and analyze the flow cytometry data. For custom code that has been deposited into a community repository, provide accession details.</i>
Cell population abundance	<i>Describe the abundance of the relevant cell populations within post-sort fractions, providing details on the purity of the samples and how it was determined.</i>
Gating strategy	<i>Describe the gating strategy used for all relevant experiments, specifying the preliminary FSC/SSC gates of the starting cell population, indicating where boundaries between "positive" and "negative" staining cell populations are defined.</i>

Tick this box to confirm that a figure exemplifying the gating strategy is provided in the Supplementary Information.

Magnetic resonance imaging

Experimental design

Design type	Indicate task or resting state; event-related or block design.
Design specifications	Specify the number of blocks, trials or experimental units per session and/or subject, and specify the length of each trial or block (if trials are blocked) and interval between trials.
Behavioral performance measures	State number and/or type of variables recorded (e.g. correct button press, response time) and what statistics were used to establish that the subjects were performing the task as expected (e.g. mean, range, and/or standard deviation across subjects).

Acquisition

Imaging type(s)	Specify: functional, structural, diffusion, perfusion.
Field strength	Specify in Tesla
Sequence & imaging parameters	Specify the pulse sequence type (gradient echo, spin echo, etc.), imaging type (EPI, spiral, etc.), field of view, matrix size, slice thickness, orientation and TE/TR/flip angle.
Area of acquisition	State whether a whole brain scan was used OR define the area of acquisition, describing how the region was determined.
Diffusion MRI	<input type="checkbox"/> Used <input type="checkbox"/> Not used

Preprocessing

Preprocessing software	Provide detail on software version and revision number and on specific parameters (model/functions, brain extraction, segmentation, smoothing kernel size, etc.).
Normalization	If data were normalized/standardized, describe the approach(es): specify linear or non-linear and define image types used for transformation OR indicate that data were not normalized and explain rationale for lack of normalization.
Normalization template	Describe the template used for normalization/transformation, specifying subject space or group standardized space (e.g. original Talairach, MNI305, ICBM152) OR indicate that the data were not normalized.
Noise and artifact removal	Describe your procedure(s) for artifact and structured noise removal, specifying motion parameters, tissue signals and physiological signals (heart rate, respiration).
Volume censoring	Define your software and/or method and criteria for volume censoring, and state the extent of such censoring.

Statistical modeling & inference

Model type and settings	Specify type (mass univariate, multivariate, RSA, predictive, etc.) and describe essential details of the model at the first and second levels (e.g. fixed, random or mixed effects; drift or auto-correlation).
Effect(s) tested	Define precise effect in terms of the task or stimulus conditions instead of psychological concepts and indicate whether ANOVA or factorial designs were used.
Specify type of analysis:	<input type="checkbox"/> Whole brain <input type="checkbox"/> ROI-based <input type="checkbox"/> Both
Statistic type for inference (See Eklund et al. 2016)	Specify voxel-wise or cluster-wise and report all relevant parameters for cluster-wise methods.
Correction	Describe the type of correction and how it is obtained for multiple comparisons (e.g. FWE, FDR, permutation or Monte Carlo).

Models & analysis

n/a	Involvement in the study
<input type="checkbox"/>	<input type="checkbox"/> Functional and/or effective connectivity
<input type="checkbox"/>	<input type="checkbox"/> Graph analysis
<input type="checkbox"/>	<input type="checkbox"/> Multivariate modeling or predictive analysis
Functional and/or effective connectivity	Report the measures of dependence used and the model details (e.g. Pearson correlation, partial correlation, mutual information).
Graph analysis	Report the dependent variable and connectivity measure, specifying weighted graph or binarized graph, subject- or group-level, and the global and/or node summaries used (e.g. clustering coefficient, efficiency, etc.).

